Deformable MEMS grating for wide tunability and high operating speed

Maurizio Tormen(1), Yves-Alain Peter(2), Philippe Niedermann(1), Arno Hoogerwerf(1), Herbert Shea(3) and Ross Stanley(1)

1 Centre Suisse d'Electronique et de Microtechnique SA, Rue Jaquet-Droz 1, 2007 Neuchâtel, Switzerland
E-mail: maurizio.tormen@csem.ch
2 Département de Génie Physique, Ecole Polytechnique de Montréal, Montréal, Canada
3 Microsystems for Space Technologies Laboratory (IMM-LMTS), EPFL, Lausanne, Switzerland

ABSTRACT

Diffractive MEMS are interesting for a wide range of applications, including displays, scanners or switching elements. Their advantages are compactness, potentially high actuation speed and in the ability to deflect light at large angles.
We have designed and fabricated deformable diffractive MEMS grating to be used as tuning elements for external cavity lasers. The resulting device is compact, has wide tunability and a high operating speed.
The initial design is a planar grating where the beams are free-standing and attached to each other using leaf springs. Actuation is achieved through two electrostatic comb drives at either end of the grating. To prevent deformation of the free-standing grating, the device is 10 μm thick made from a Silicon on Insulator (SOI) wafer in a single mask process. At 100V a periodicity tuning of 3% has been measured. The first resonant mode of the grating is measured at 13.8 kHz, allowing high speed actuation. This combination of wide tunability and high operating speed represents state of the art in the domain of tunable MEMS filters.
In order to improve diffraction efficiency and to expand the usable wavelength range, a blazed version of the deformable MEMS grating has been designed. A key issue is maintaining the mechanical properties of the original device while providing optically smooth blazed beams. Using a process based on anisotropic KOH etching, blazed gratings have been obtained and preliminary characterization is promising.

Keywords: Optical MEMS, MEMS Grating, Diffractive MEMS, Tunable laser

MOEMS Display, Imaging, and Miniaturized Microsystems IV, edited by Hakan Ürey,
David L. Dickensheets, Bishnu P. Gogoi, Proceedings of SPIE Vol. 6114,
61140C, (2006) · 0277-786X/06/$15 · doi: 10.1117/12.644523

1. Introduction

In Optical MEMS, the family of diffractive MEMS is interesting for a wide range of applications where more standard optical MEMS, in particular tilting mirrors [1]-[3], are currently used. The advantages of diffractive MEMS are compactness, potentially high actuation speeds, the ability to deflect light at large angle and dynamically filtering light with narrow spectral responses. Different application fields are currently looking at diffractive MEMS [1], such as information technology (e.g. projection displays, barcode readers, retina scanning readers), medicine (e.g. endoscopes), telecommunication (e.g. optical switch, wavelength tuning, variable optical attenuator), metrology (e.g. 3D shape measuring, spectroscopy), lithography (e.g. programmable masks), astronomy (e.g. wavefront correction). Commercially available diffractive MEMS devices are used in displays, in spectroscopy and optical telecommunications [4]-[5].

Our goal is to make a compact, efficient and fast wavelength tuning to be used in external cavity lasers. The standard approach is to use a diffraction grating and an actuator to either change the grating angle, in the Littrow configuration [6], or to change the angle of light reflected back on the grating, in the Littman configuration [7]. In both cases, when the axis of mechanical motion is perpendicular to the grating [8]-[9]. When for the actuation uses MEMS structure are used, this requirement makes the structure complex. In this paper, wavelength tuning is achieved by stretching the grating along its length. The advantage of using MEMS technology in such an approach are (a) the flexibility of the grating can be tailored by mechanical design and is not limited to the material properties as in the case of a solid grating, (b) flexible elements (springs) and diffracting elements can be designed separately, (c) because diffraction gratings are interferometric systems, wavelength scale motion can have large effect optically allowing stiff devices with high resonance frequencies.

The challenges of this approach are that (a) the grating must be free standing – it must be rigid enough to be held by floating anchor points, but flexible enough to be actuated, (b) the springs need to be identical otherwise the grating will distort unevenly lowering its efficiency and wavelength selectivity, (c) the diffracting beams need to be prevented from distorting either through bending in the plane of the structure or out of plane buckling or rotation, and (d) optical quality of the optical surfaces needs to be sufficiently high, i.e. very flat surfaces are required.

First we studied the fabrication and operation of a planar deformable grating. Due to its square profile the diffraction efficiency into any given order is quite low, but has a period suitable for use with mid-infrared (5 μm) Quantum-Cascade Lasers. In order to use these deformable gratings at shorter wavelengths then either the structure has to be scaled down, in which case rigidity is lost, or they have to be used in a high order, in which case the grating needs to be blazed. A technique for creating blazed gratings is outlined in the second part of the paper.

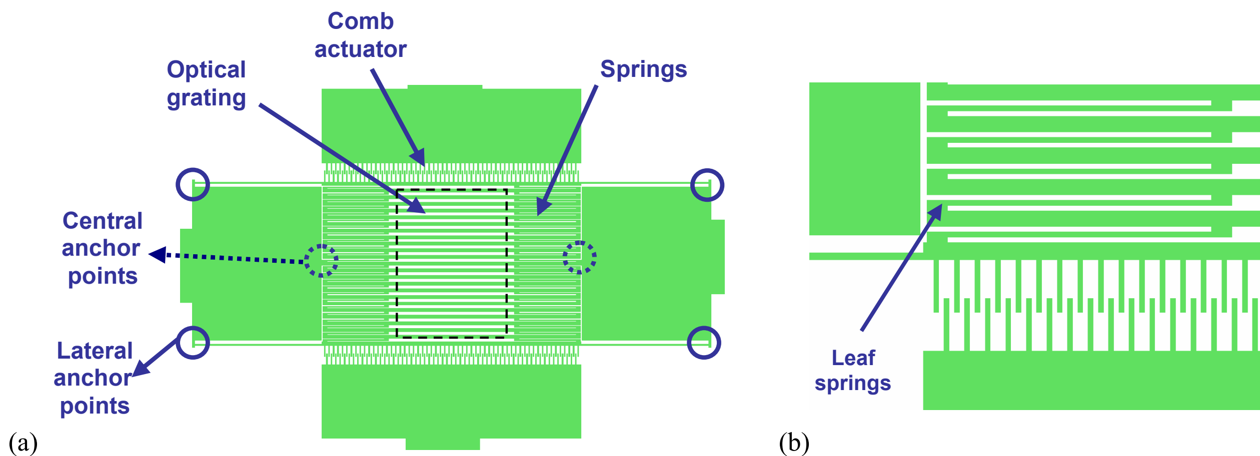

Figure 1. *(a) Overview of the deformable MEMS grating structure: it is possible to distinguish the beams forming the grating (inside the dotted area), the 6 anchor points at which the suspended structure is fixed and the comb actuators on both grating sides. The grating dimensions are on the order of 200 μm x 200 μm. (b) Detail of the deformable MEMS grating, in particular of the leaf hinge structures. The leaf hinge is formed by a thin flexible beam with two wide structures at its extremities: this structure provides the required spring constant without inducing any stress on the adjacent beams.*

2. Planar deformable MEMS grating

Two versions of deformable MEMS gratings were studied, a planar version and a blazed one. In this section, the planar one is presented, with details on its design, process flow and fabrication, mechanical and optical characterizations.

2.1. Design

Figure 1(a) shows the layout of the deformable MEMS grating. The optical grating is formed by silicon beams etched in the device layer of an SOI wafer. The grating is designed with a duty-cycle of 50% and different periods, Λ (6 μm, 9 μm and 12 μm). The grating beams, connected one to the other through grating springs, form a suspended structure that is anchored to the substrate via the oxide layer in 6 different points: the grating is held at either end at two points through flexible suspension beams which allow for a stretching motion of the grating; the grating is rigidly held in the middle by the central beam which is attached to the central anchor pads. The grating springs design is that of a leaf spring (Figure 1b). During actuation these are the only elements where stress is concentrated and, thus, where deformation is present. They do not allow torsional movement to the grating beams around their longitudinal axes. The grating is stretched by two comb actuators. The device layer thickness is 10 μm. This guarantees sufficient stiffness to the wide suspended structure to prevent stiction during the process release step and to prevent buckling during operation.
This design requires only one mask level for the definition of the grating, the springs and the actuators.

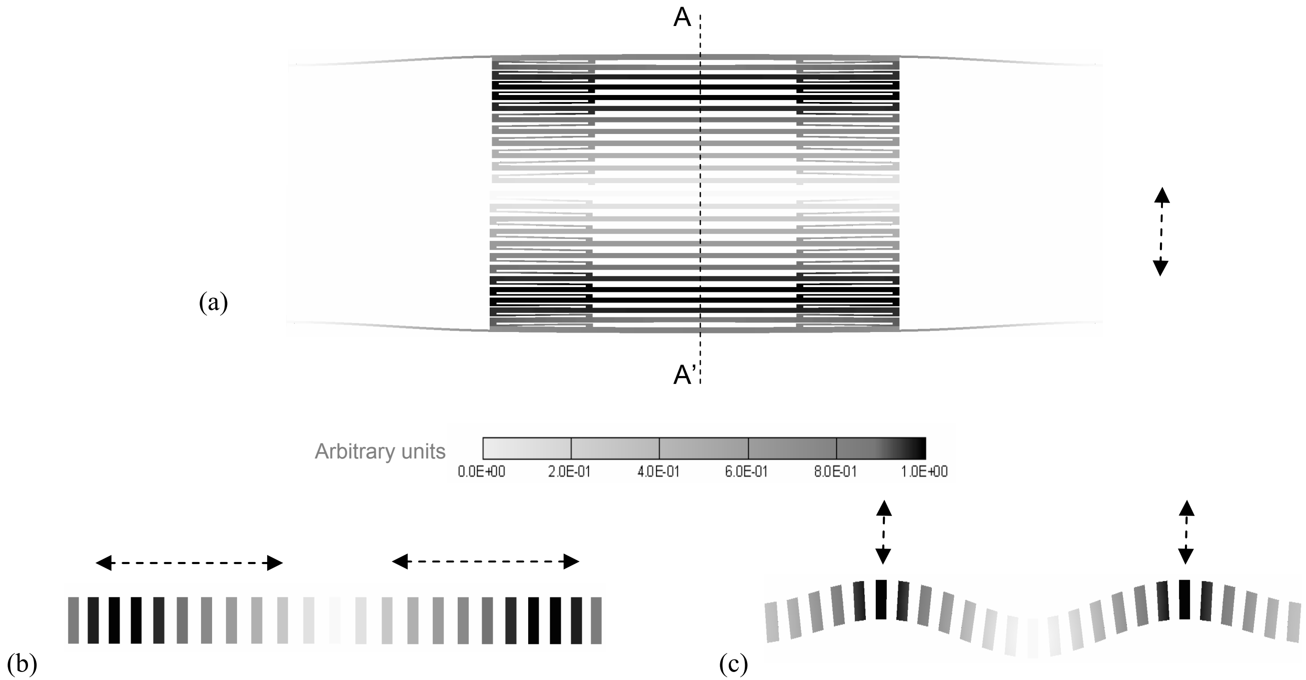

Figure 2. *(a) First (in-plane) resonant mode for the deformable MEMS grating with periodicity of 9 μm. (b) Cross-section A-A' of the structure in Figure 3(a) for the first (in-plane) resonant mode. (c) Cross-section A-A' of the structure in Figure 3(a) for the second (out-of-plane) resonant mode.*

Finite element modeling (CoventorWare^{TM}) was used to simulate the in-plane grating motion and the resonant modes of the structure. From this modeling, the first resonant mode for a structure with a 9 μm periodicity is expected at 19.5 kHz and it is in-plane; the second and third modes are expected at 40 kHz and 45 kHz and are out-of-plane modes.
Figure 2(a) shows the simulation of the first (in-plane) resonant mode seen from above. The relative motion of the beams can be seen as a cross section in Figures 3(b) and 3(c) which show the first and second (out-of-plane) resonant modes respectively.
The simulations for the structure with a 12 μm periodicity give the first three resonant modes at 28.5, 60 and 68.5 kHz, respectively. As for the 9 μm period structure, the first mode is an in-plane mode, while the second and third ones are

out-of-plane. The high frequencies of the resonant modes are obtained because of the particular structure design (in particular the spring region) and to the thickness of the device layer (10 µm).

2.2. Fabrication

Figure 3 shows the process flow for planar deformable MEMS gratings. The process starts with a low resistivity SOI (Silicon On Insulator) wafer (Figure 3a) with a 2 µm buried oxide layer and a p++ 10 µm device layer. This thickness ensures that the structure is stiff enough to prevent stiction during the final release step.

Photolithography (Figure 3b) with 1 µm minimum feature size defines structures. It is followed by deep reactive ion etching (Figure 3c) to define in one step grating beams, springs and comb actuators. A well controlled lithography and deep reactive ion etching are required in order to guarantee that all flexible structures have the same spring constant. The accuracy of the positioning of each grating beam depends on such a control. The device is then released by removing the sacrificial oxide in HF vapor (Figure 3d) [10]. A final coating step can be added (e.g. a gold coating) to give the required reflection properties for any specific spectral region.

Gratings with period of 6 µm, 9 µm and 12 µm were fabricated on the same wafer. Figure 4(a) and 4(b) show the top view of an entire device and a cross-section of the spring region, respectively, for a device with 6 µm period on a Silicon test wafer.

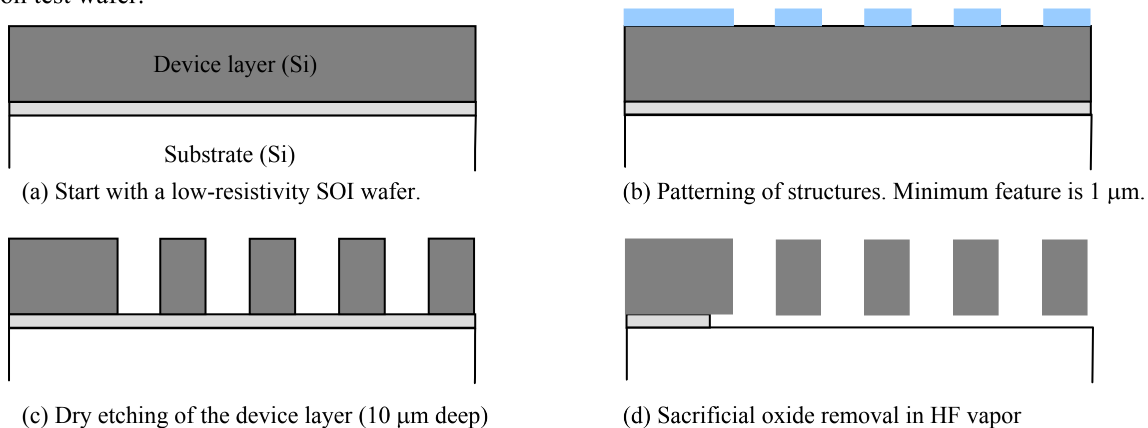

Figure 3. *Process flow for the deformable MEMS grating fabrication*.

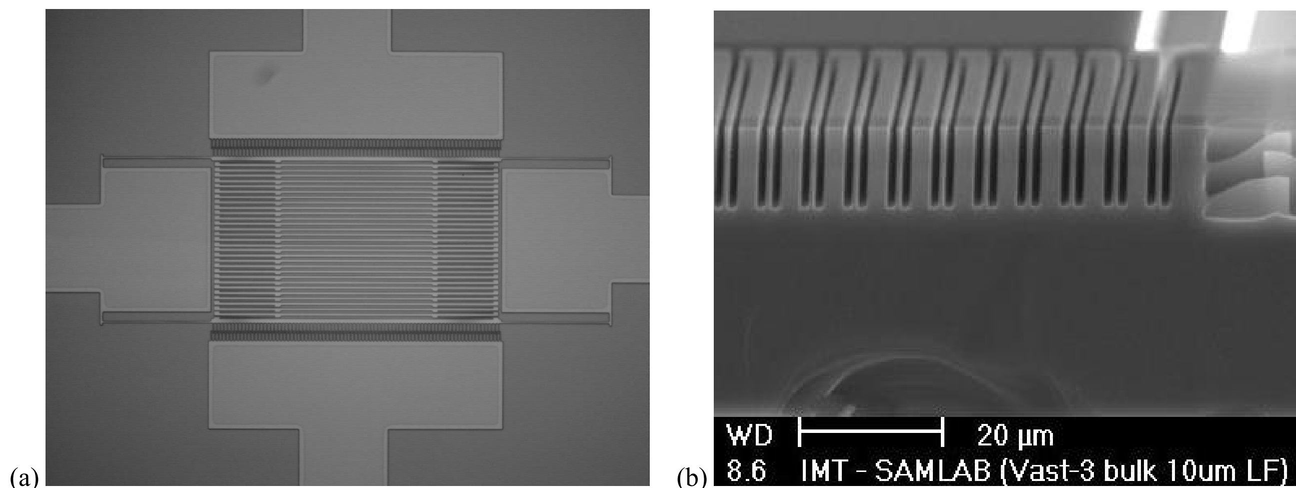

Figure 4. *Fabricated devices on a Si test wafer. (a) Top View of an entire device (optical microscope). (b) Cross-section SEM image of the spring region for one test structure with 6 µm period.*

2.3. Mechanical characterization

The deformable gratings were tested by measuring the displacement as a function of the applied voltage and by measuring the resonant frequencies of the structure using a Doppler Interferometer. The displacement was measured in a probe station by applying a voltage to the comb actuators. Figure 5 shows a detailed view of a grating with a 9 μm period (a) with no applied voltage and (b) with 100 V applied. In the latter case each end of the grating moves by 3.1 μm, resulting in an overall stretching of the structure of 6.2 μm. This is equivalent to a relative tuning of the grating period $\Delta\Lambda/\Lambda$ of approximately 3% or to a tuning range of 150 nm at the wavelength of interest, 5 μm.
In this measurement, maximum displacement was limited by the high voltage supply: in principle the present structure can have a relative tuning $\Delta\Lambda/\Lambda$ up to 10%, the limiting factor being the comb dimension.

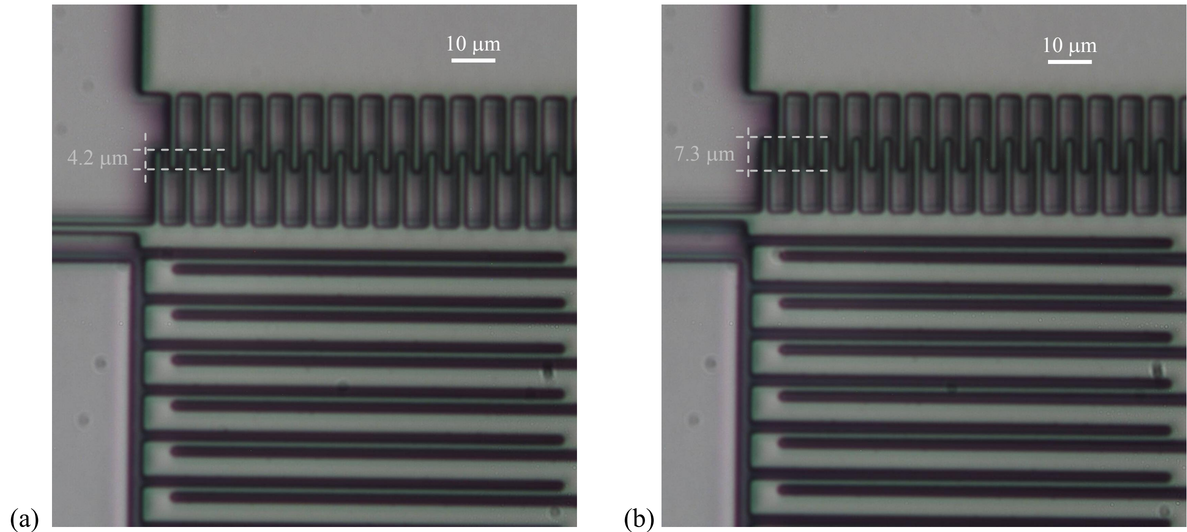

Figure 5. *Top view of the electrostatic comb drive and spring region for two different actuation voltages: (a) no applied voltage; (b) 100V applied. The displacement of the end of the grating is 3.1 μm.*

Figure 6 shows the measured displacement of the comb actuator versus the applied voltage. Experimentally, a linear behavior of the displacement is found at higher voltages. A quadratic behavior is normally expected from this kind of structure, but FEM simulations of the entire structure agree experiment.
The deviation from the ideal quadratic behavior is related to the mechanical properties of the flexible anchor beams, on which the structure is suspended (Figure 1). In fact the flexible anchor beams are not free to rotate around the axis that is perpendicular to the suspended structure plane and that passes through the anchor point itself. Figure 7(a) shows that with the current design, the stress is concentrated in the beam, but not in the anchor support. This linear behavior reduces the range of displacement but could help in simplifying any controlling algorithms for the actuation.
If needed, the mechanical constraint can be removed by adding a right-angle in the beam at the anchor support, enabling the full exploitation of the applied voltage: Figure 7(b) shows such an anchor support design and simulation shows that this structure has an ideal quadratic behavior. In this case, in fact, the anchor beam can rotate freely around the anchor point: this behavior can be deduced by the stress distribution that is not only in the flexible anchor beam but in the anchor support as well.

The frequencies for the first two resonant modes of the structure with periodicity of 9 μm were measured using a Doppler Interferometer that is able to measure the out-of-plane displacement of a structure driven with sinusoidal voltage at a frequency spanning a desired range.
Figure 8(a) reports the out-of-plane displacement as a function of frequency. Two resonances can be seen, the first at 13.8 kHz (f1) and the second at 28.1 kHz (f2). The first mode should not normally be present in an out-of-plane displacement (Figure 2a and 2b). However, a small coupling of the in-plane resonant mode to vertical displacement makes it appear in the Doppler measurement. Figure 8(b) shows the out-of plane motion of the whole structure for the

second resonant mode (28.1 kHz). This corresponds to the second resonant mode of the structure (out-of-plane mode) as simulations have shown (Figure 2b).
The experimental values for the first two modes (f1=13.8 and f2=28.1 kHz) can be compared with the simulated ones (19.5 and 40 kHz). The relative positions of resonant modes agree, even if a discrepancy exists in the absolute values. Such discrepancy is probably due to the tolerances in the process that were not taken into account in the simulations and will be further investigated. While the resonant frequencies are lower than expected they are still high enough to allow sub-millisecond tuning of the grating over its full range.

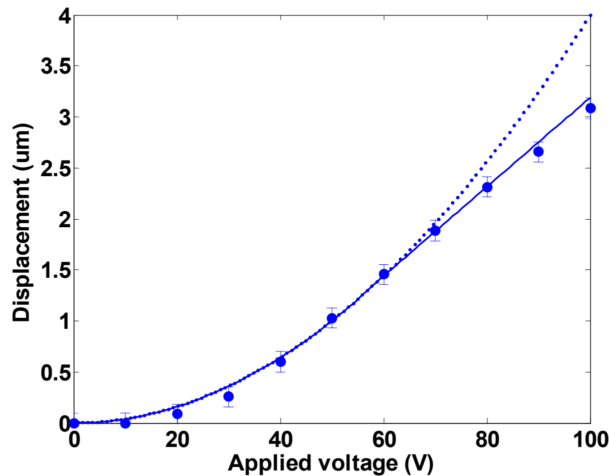

Figure 6. *Measured (dots) and simulated (solid line) displacement versus applied voltage for the 9 μm period grating. Maximum displacement at each grating end is 3.1 μm. Good agreement is obtained with simulated behavior. A deviation from ideal quadratic behavior (dotted line) is related to the design of the anchor points.*

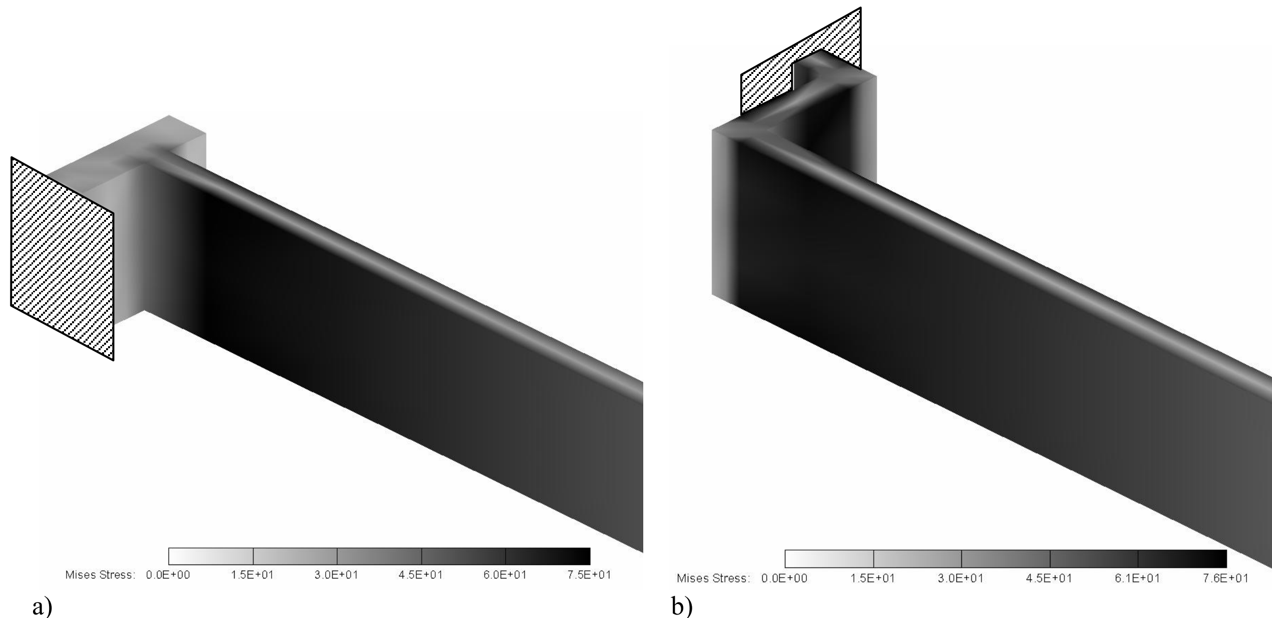

Figure 7. *(a) Simulation of the stress for the actual lateral anchor support when 120V are applied to the comb actuators. In this case the stress is concentrated in the flexible anchor beam and a linear regime is obtained in the actuation. (b) Simulation of the stress in a lateral anchor with 120V applied to the comb actuators, allowing the actuation to follow the ideal quadratic behavior. Mises Stresses are in Mpa.*

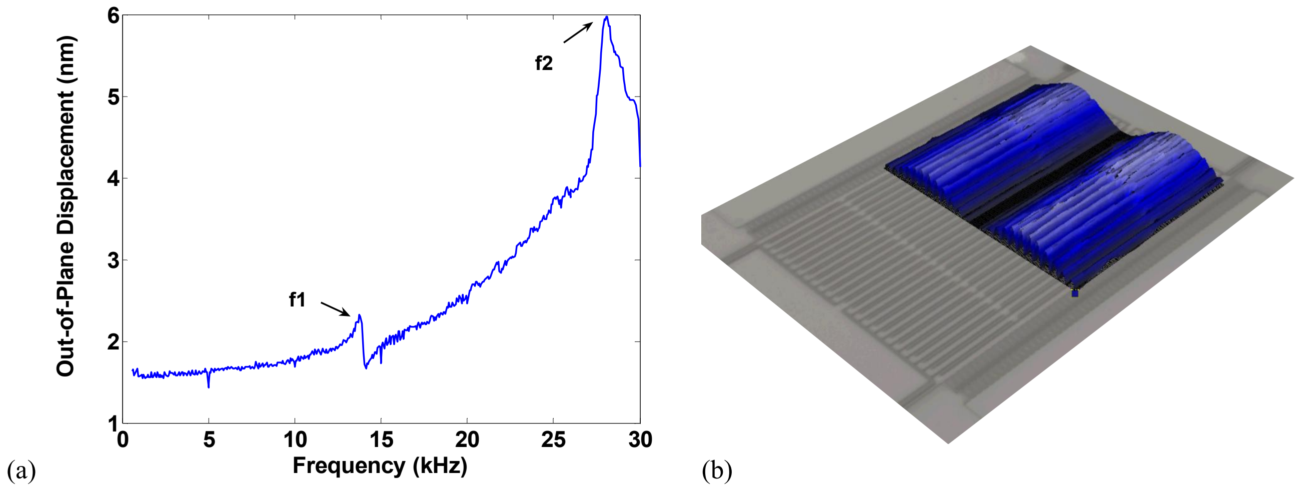

Figure 8. *(a) Doppler Interferometer measurement of the first and second resonant mode frequencies for the structure with periodicity of 9 μm. They are located at 13.8 kHz and 28.1 kHz, respectively. (b) Experimentally measured resonant mode of the structure when resonating at 28.1 kHz.*

2.4. Optical characterization

The fabricated structures were tested optically with a He-Ne laser (632.8 nm) in a static condition.
Figure 9(a) shows the diffraction intensity as a function of angle for a grating with period 12 μm at normal incidence. Good agreement is found between the experimental results and the optical simulations in which the geometrical parameters of the grating are derived from direct measurement: in particular, the grating duty cycle is not 0.5 as designed, but 0.45 (Figure 9b).
In order to use such a grating to tune external cavity lasers, diffraction efficiency can be improved by blazing the grating beams.

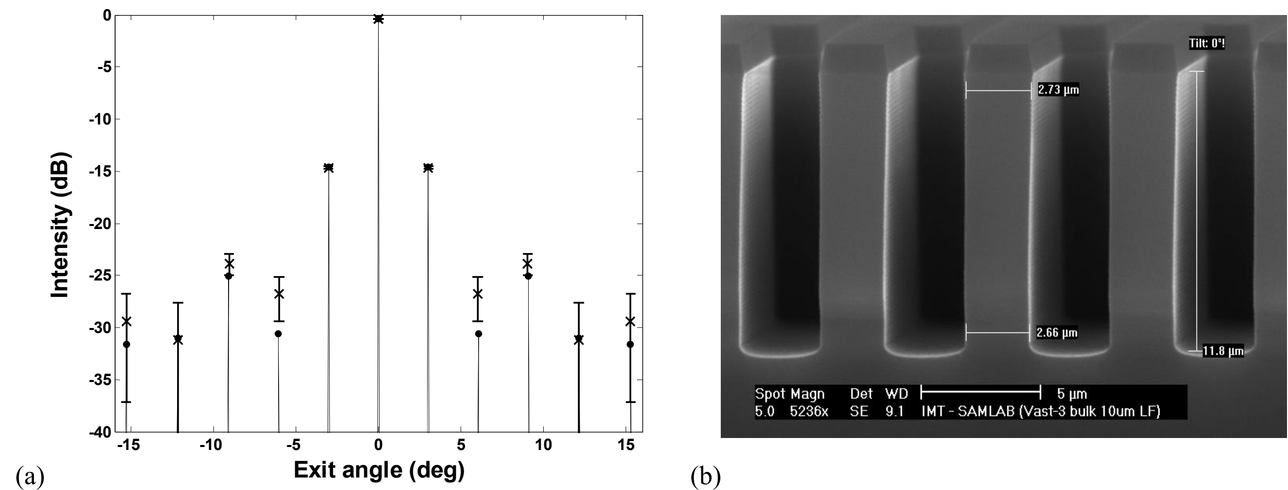

Figure 9. *(a) Intensity of diffracted orders for the 12 μm period grating at normal incidence at the He-Ne laser wavelength of 632.8 nm. Good agreement is obtained between experiments and optical simulations using data derived from geometrical characterization. (b) Geometrical characterization of the 12 μm period grating (SEM cross-section in a test wafer).*

3. Blazed deformable MEMS grating

In order to improve diffraction efficiency, the blazed version of the deformable MEMS gratings is introduced. Moreover, since the blazed grating is used in a high order, it allows operation at shorter wavelengths without the scaling down of the structure, in which case rigidity would be lost.

In the present section, the blazed deformable MEMS gratings are presented, with details on its design, process flow and preliminary fabrication results.

3.1. Design

For the blazed gratings, the basic layout is the same used for the planar ones. Only the process flow is modified with the introduction of extra fabrication steps and a second mask. The challenge for blazed gratings is to obtain an optically smooth surface. Anisotropic KOH etching is well known for its ability to stop at {1 1 1} Silicon planes, e.g. silicon v-grooves. This technique was chosen, which provides optically smooth surfaces but fixes the blaze angle at 54.74°.

The second mask is introduced in order to apply the steps needed to obtain the blazed features only in the beam region: this region correspond to the dotted region in Figure 1(a).

A commercial KOH etch simulation tool was used to verify the expected the structure of the etched beam and to verify how much the KOH etches the beam in the mask border region (Figure 10a). The particular shape of the etched beam is a consequence of the KOH angle and the exposure angle at the lithographic step (see 3.2). The second small tilted side is not desired, but at the same time it doesn't represent a problem since the grating will be operated in the Littrow condition (Figure 10b), that is the input angle (in respect to the vertical plane) is equal to the blazing angle (in respect to the horizontal plane). In such a case the second small tilted side is shadowed completely by the adjacent beam.

From Figure 10(b), moreover, the need of a safety margin of about 10 μm can be deduced. This has been introduced between the mask border region and the spring region as seen in Figure 1(a).

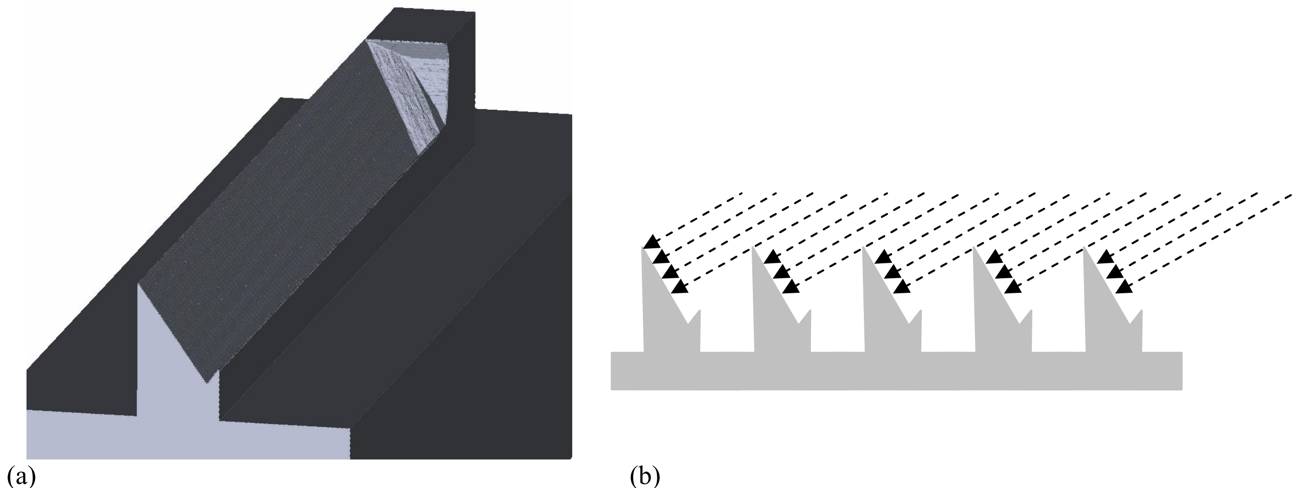

(a) (b)

Figure 10. *(a) Simulated structure of the blazed beam after KOH etch. (b) The blazed grating is supposed to be operated in the Littrow condition.*

3.2. Fabrication

Figure 11 shows the process flow that has been used for the fabrication of the blazed deformable MEMS gratings.

Steps (d) to (h) were added to the process used for the planar deformable MEMS grating presented in 2.2.

The proposed process is thus fully compatible with the process for the planar gratings, giving the possibility to use the same fabrication run to obtain both the planar and the blazed deformable MEMS grating, even on the same wafer.

After the deep reactive ion etching that defines grating beams, springs and comb actuators (c), a thermal oxide is grown and a resist spinned on the wafer (d): the oxide, conveniently patterned, will act as mask during the KOH etch.

In order to pattern the oxide only in the region of interest, a mask is used at an exposure angle of 30 degrees (e). After resist development (f), a BHF etch (g) is applied to remove the oxide specifically in the regions where the KOH bath has to etch the Silicon beams (h). The device is then exposed to HF vapor (i) to remove the thermally grown oxide and to liberate the grating, by removing the sacrificial oxide.

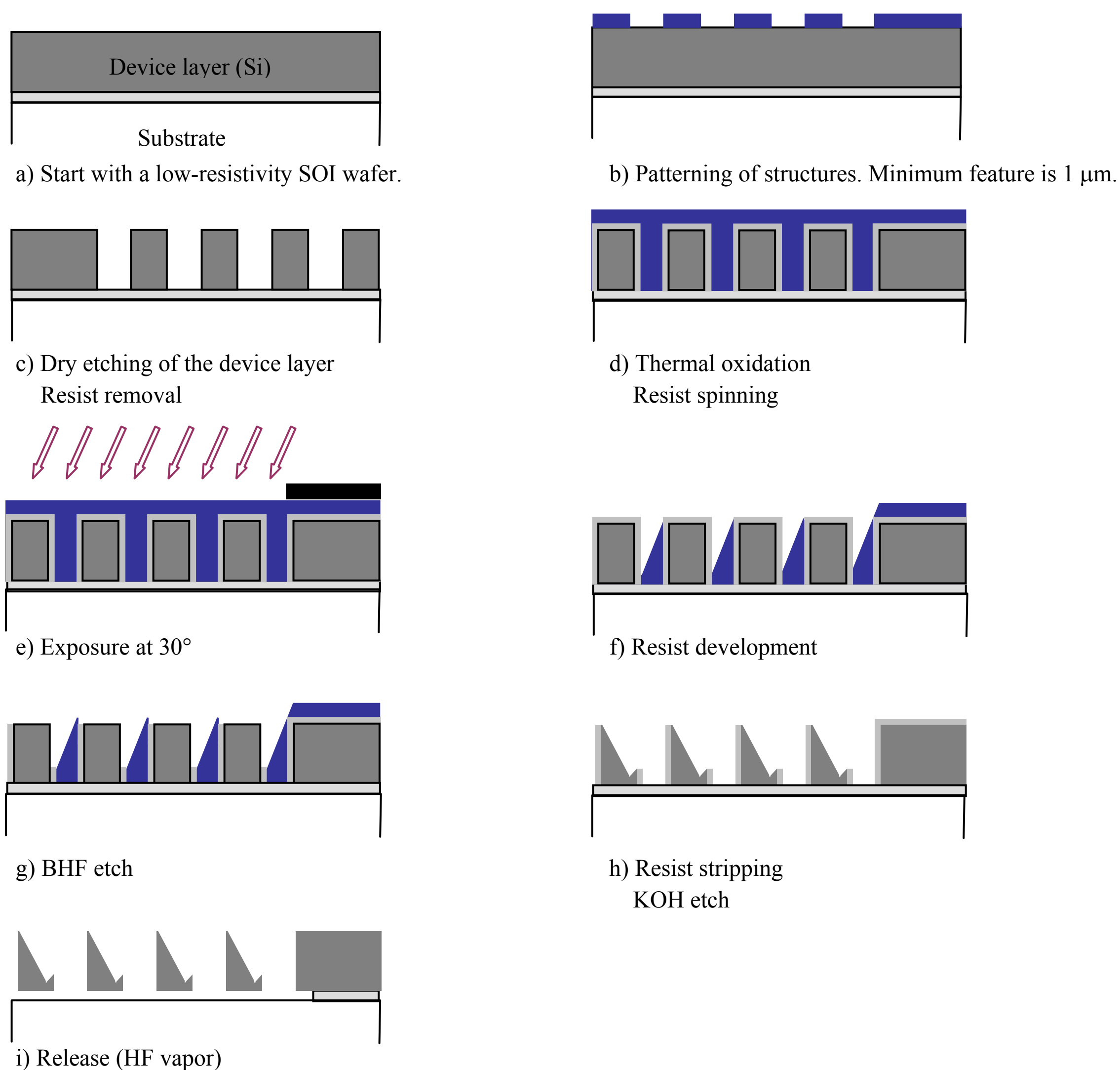

Figure 11. *Process flow for the blazed deformable MEMS gratings. This process adds steps (d) to (h) to the process for the planar deformable MEMS gratings (Figure 3). Using KOH etch, an optically smooth surfaces can be obtained, corresponding to {1 1 1} Silicon planes. The entire process requires two masks.*

The feasibility of the process has been verified. Figure 12 presents preliminary fabrication results: in (a) the top view of a grating test structure, in (b) the lateral view. It was possible to obtain the desired structure as shown by the good agreement with simulations results.
In (b) the lateral residuals of the oxide after the KOH step are still visible. They will be removed by the final HF vapor release step.

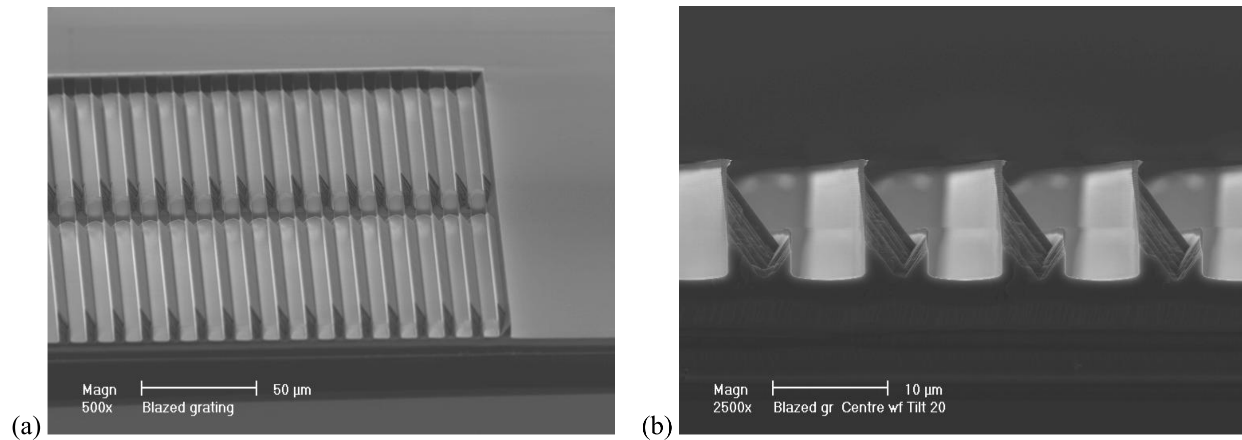

(a) (b)

Figure 12. (*a) Top view of a grating test structure with periodicity 12 µm. (b)Llateral view of the same test structure.*

4. Conclusions

Planar deformable MEMS gratings were designed, fabricated, mechanically and optically tested. Good agreement between experimental results and expected performances was obtained. Moreover, the feasibility for blazed deformable MEMS gratings was demonstrated.

If compared to the state of the art, this approach extends both the tuning range and the operational frequency range of existing MEMS diffraction grating.

In fact high actuation speed can be obtained through a piezoelectric actuation mechanism [11]-[12], but in this case a small tuning range is obtained (relative tuning $\Delta\Lambda/\Lambda$ of 0.2% was achieved). On the other hand, if a thermal actuation mechanism is used [13], a wider tuning range can be achieved, but the actuation speed cannot be higher than some hundreds of Hz.

Other advantages of the present approach are:

- Only standard fabrication steps are required. In particular, in both versions (planar gratings and blazed ones) the minimum feature is 1 µm wide, not requiring special and expensive lithographic equipment.
- A minimum number of masks is required: a single mask is needed in fact for the planar gratings, two for the blazed ones.
- In both versions (planar gratings and blazed ones), the surface quality that can be obtained is superior if compared to side etching approach: in fact the grating surface is either the top surface of an SOI wafer or the {1 1 1} Silicon planes.

The device will be used, in its blazed version, as a tunable element in mid-IR (5 µm) external cavity Quantum Cascade lasers.

ACKNOWLEDGEMENTS

This work was partly funded by the Swiss NCCR Quantum Photonics program. We thank them for their support. We thank Dr. Simon Henein for fruitful discussions on the spring design. The devices were fabricated in the clean rooms of COMLAB, the shared facilities of the Institute of Microtechnology, University of Neuchatel, and CSEM.

REFERENCES

1. Schenk H. et al. “Photonic microsystems: an enabling technology for light deflection and modulation”; Proceedings of the SPIE, v 5348, n 1, 2004, pp 7-21
2. Van Kessel P.F. et al. “A MEMS-based projection display” Proceedings of the IEEE Vol. 86, n 8, Aug. 1998 pp 1687-1704
3. Peter Dürr et al. “Micromirror spatial light modulators”, Proceedings of MOEMS '99, 1999, pp.60-65.
4. www.siliconlight.com
5. www.polychromix.com/html/products.htm
6. Flemming M.W. et al., IEEE J.Quantum Electronics 17, 44 (1981)

7. Littman M.G. et al. “Continuous single-mode scanning of tunable lasers: a new approach”; CLEO '81. Conference on Lasers and Electro-Optics 1981, p 82
8. Syms, R.R.A. et al. “MOEMS tuning element for a Littrow external cavity laser”, Journal of Microelectromechanical Systems, v 12, n 6, Dec. 2003, p 921-8
9. http://www.iolon.com/apollo.html
10. Overstolz, T et al. “A clean wafer-scale chip-release process without dicing based on vapor phase etching”, Micro Electro Mechanical Systems, 2004. 17th IEEE International Conference on MEMS – 2004, p 717 - 720
11. Chee W. et al., “Analog tunable gratings driven by thin-film piezoelectric microelectromechanical actuators”, Applied Optics, v 42, n 4, 1 Feb. 2003, p 621-6
12. Chee W. et al., “Analog piezoelectric-driven tunable gratings with nanometer resolution”, J. Microel. Systems, v 13, n 6, Dec. 2004, p 998-1000
13. Zhang, X.M., Liu, A.Q. “A MEMS pitch-tunable grating add/drop multiplexers”, Optical MEMS 2000, 21-24 Aug. 2000 pp 25-26